Received: 5 May 2019 | Revised: 26 July 2019 | Accepted: 29 July 2019 | Published on: 15 October 2019

DOI: 10.1002/asna.201913660

Astronomische Nachrichten

ORIGINAL ARTICLE

Kilonova afterglow rate from spherical and axisymmetrical models

J. Kóbori

Department of Physics of Complex Systems, Eötvös Loránd University, Budapest, Hungary

Correspondence
J. Kóbori, Department of Physics of Complex Systems, Eötvös Loránd University, Budapest, Hungary.
Email: jkobori@caesar.elte.hu

Present Address:
J. Kóbori, 1/A Pázmány Péter Sétány, 1117, Budapest, Hungary.

Abstract

Detecting the afterglows of double-neutron star merger events is a challenging task because of the quick fading of the observed flux. In order to create an efficient observing strategy for their observing method, it is crucial to know their intrinsic rate. Unfortunately, the numerous models existing today predict this rate on a very wide range. Our goal in this paper is to compare the different levels of approximations in order to determine their reliability. We find that there is a significant discrepancy in the expected detection rate between the spherical and axisymmetrical models ($\sim$18 and $\lesssim 1$ yr^{-1}, respectively). In addition, choosing different models for the input parameters (for example, redshift and time delay distribution) has also a strong effect on the results.

KEYWORDS

gamma rays: bursts, methods: numerical, methods: statistical

1 | INTRODUCTION

The first joint discovery of the GW 170817 gravitational wave source (Abbott et al. 2017a) and the GRB 170817A (Abbott et al. 2017b) with its kilonova (KNe) afterglow (Soares-Santos et al. 2017) was a major step in the era of multimessenger astronomy. The detection of the multi-waveband afterglow allowed detailed modeling of the kilonova physics, so that the parameters shaping the resulting light curves could be calculated.

Having an efficient observing strategy for a sky survey program (e.g., Large Synoptic Survey Telescope (Ivezić et al. 2019)) can greatly enhance the probability to detect kilonova afterglows. There are numerous works which give an estimation for kilonova afterglow rates for the future sky surveys (e.g., Cao et al. 2018; Chruslinska et al. 2018; Cowperthwaite et al. 2019; Dominik et al. 2013; Eldridge et al. 2019; Jin et al. 2018; Kruckow et al. 2018; Mapelli & Giacobbo 2018; Pol et al. 2019; Sadowski et al. 2008; Scolnic et al. 2018; Sun et al. 2015; Tan et al. 2018; Vigna-Gómez et al. 2018; Wollaeger et al. 2018). When calculating these rates, one has to take into account the short gamma-ray burst (sGRB) rate determined from observations (e.g., Coward et al. 2012; Dietz 2011; Paul 2018; Petrillo et al. 2013; Ruffini et al. 2018; Sun et al. 2015; Wanderman & Piran 2015; Yonetoku et al. 2014; Zhang & Wang 2018) or from population synthesis methods (e.g., Belczynski et al. 2016; Bogomazov et al. 2007; Chruslinska et al. 2018; Nakar et al. 2006; Saleem et al. 2018b; Ziosi et al. 2014). In addition, the particular afterglow model (e.g., composition and structure) employed in the study can significantly affect the results.

In 1993, it was discovered by Kouveliotou et al. 1993 that GRBs, based on their duration, can be divided into two groups: short- and long-duration bursts. The progenitor objects of long GRBs were thought to be core collapse supernovae (Woosley 1993). This idea was supported by the observations: they typically occur in star forming regions in their host galaxies (e.g., Bloom et al. 2002; Christensen

et al. 2004), and in some cases type Ic supernovae have been detected in the bursts' spectra (e.g., Galama et al. 1998; Hjorth et al. 2003). The short bursts were associated with compact object mergers (Eichler et al. 1989; Narayan et al. 1992). This was supported by the observations of the Swift satellite: a fraction of these bursts are located in elliptical galaxies (with old stellar population), and they are less energetic on average and occur at lower redshifts (Fox et al. 2005; Gehrels et al. 2005). Also, Balázs et al. (2003) applying statistical tests to the observational data showed that the short and long GRBs have intrinsically different high-energy properties. The link between short GRBs and kilonovae was established by Li & Paczyński (1998). They showed that the radioactive ejecta from neutron star–neutron star/black hole merger can provide a source for powering transient events. Such an event, initially called "mini-supernova," is a distinctive signature of compact binary mergers. The first direct evidence for the kilonova–short GRB connection was presented by Tanvir et al. (2013). They reported evidence for infrared emission in excess of the afterglow radiation following the short GRB 130603B. They attributed this radiation to the accompanying kilonova event. In another two cases (GRB 050709 and GRB 060614), a similar infrared emission was observed (Jin et al. 2015; Yang et al. 2015). Observational data also indicate the presence of various subgroups of GRBs (e.g., Řípa et al. 2012; Řípa & Mészáros 2016; Virgili et al. 2013). Based on these results, we consider only short GRBs as progenitor objects of kilonovae in this article.

Recent results (e.g., Addison et al. 2018; Riess et al. 2019) suggest that the values of the Hubble constant calculated from Ia type supernovae (SN) measurements and the ones derived from the fluctuations in the cosmic microwave background significantly differ at 4σ. This so-called Hubble tension raised serious concerns about the validity of the widely accepted ΛCDM model. We discuss the effect of this discrepancy, if there is any, on the kilonova afterglow predictions we make (Section 3.4). In this paper, if not stated otherwise, we adopt the standard ΛCDM cosmological parameters $H_0 = 67.8$ km s^{-1} Mpc^{-1}, $\Omega_M = 0.308$, $\Omega_\Lambda = 0.692$ (Planck Collaboration et al. 2016).

Our aim in this work is to compare the merger rates calculated with spherical and axisymmetrical models. Moreover, the effect of using different approximations for the input parameters (e.g., redshift distribution) is investigated.

2 | LIGHTCURVE SIMULATIONS

At the beginning of this section, we describe the kilonova models we used to simulate afterglows (Section 2.1). After that, the applied redshift distributions (Section 2.3) and binary neutron star merger rates (Section 2.3) are briefly summarized.

The afterglow samples were generated with the MOSFiT Python code created by Guillochon et al. (2018). It is able to simulate light curves of various transient optical events.

2.1 | Kilonova models

Two different kilonova models were used in our calculations: a spherical one created by Villar et al. (2017) (hereafter V17), and an axisymmetrical one constructed by Perego et al. (2017) (hereafter P17).

2.1.1 | Spherical model

The simplest approximation when simulationg kilonova afterglows is to assume that the ejecta have spherical structure. Such a model, like the one created by Villar et al. (2017), usually has two or three ejecta components:

1. "Blue" ejecta: A low opacity dynamical outflow ($\kappa \approx 0.5$ cm^{-2} g^{-1}), concentrated to the polar regions, produced by the shock from the collision between the merging neutron stars.
2. "Purple" ejecta: A mass component with moderate ($\kappa \approx 3$ cm^{-2} g^{-1}) opacity, originated from the accretion disk.
3. "Red" ejecta: A high opacity component ($\kappa \approx 10$ cm^{-2} g^{-1}) due to the lanthanide-rich material.

The luminosity produced by the radioactive decay of formerly generated r-process nuclei is partially converted into the observed flux. Fitting the light curve of the GW170817 event V17 suggests that it is adequately described with the three component model. Thus, in our work, we simulate KNe afterglows with the three ejecta model. The ranges for the input parameters were taken from Della Valle et al. (2018).

2.1.2 | Axisymmetrical model

In order to make the KNe afterglow model more realistic, we implemented an axisymmetric ejecta structure created by Perego et al. (2017) into the MOSFiT code. The difference to the spherical model is that the mass and the opacity has a specific angular distribution. Like the spherical model, it has three ejecta components:

1. Dynamical (blue): The mass distribution can be approximated by $F(\theta) = \sin^2\theta$.
2. Wind (red): Most likely polar emission with uniform distribution in mass, $F(\theta) \approx$ const for $\theta \lesssim \theta_w \approx \pi/3$.
3. Secular (purple): Equatorial-dominated flow, $F(\theta) = \sin^2\theta$

where $F(\theta)$ characterizes the mass distribution according to

$$m_{ej} = \sum_{k=1}^{12} m_{ej,k} = \sum_{k=1}^{12} 2\pi \int_{\theta_k - \Delta\theta/2}^{\theta_k + \Delta\theta/2} F(\theta)\sin(\theta) d\theta \quad (1)$$

TABLE 1 The allowed ranges for the kilonova (KNe) input parameters

Parameter	P17 Range	V17 Range	Ours Range
$m_{\rm ej,\ d/blue}$	0.05–5	0.5–2	0.5–5
$m_{\rm ej,\ purple}$	$0.05 \times M_{\rm disk}$	1–5	0.001–4
$m_{\rm ej,\ red}$	$<0.03 \times M_{\rm disk}$	0.5–2	0.001–8
$v_{\rm rms,\ d}$	0.1–0.23	0.25	0.1–0.3
$v_{\rm rms,\ w}$	0.33–0.67	0.15	0.01–0.07
$v_{\rm rms,\ s}$	0.017–0.04	0.15	0.01–0.07
$\kappa_{\rm d}$	0.5–30	0.5	0.1–5
$\kappa_{\rm w}$	0.5–1	30	5–10
$\kappa_{\rm s}$	1–30	10	10–30

Note: The $M_{\rm disk}$ indicates the mass of the disk produced by the massive neutron star before collapsing into a black hole. It has a range of $10^{-2}M_{\odot} < M_{\rm disk} < 10^{-1}M_{\odot}$. The mass is in unit of $10^{-2}M_{\odot}$, the speed is in c, and the opacity is in $\rm cm^{-2}\ g^{-1}$.

Two different parameter sets were applied to the P17 model: (a) the one used by Perego et al. (2017) to infer the physical parameters of the event AT 2017gfo and a "custom" one and (b) where we collected the parameters generally used in the literature. The parameter ranges for the different cases are listed in Table 1.

2.2 | Redshift distribution

When simulating short GRBs two different factors should be considered regarding the redshift parameter: the intrinsic redshift distribution of the progenitor compact merger system and the time delay between the formation of the system and the inspiral. Unlike in the case of the long GRBs where the observed redshift distribution more or less follows the cosmic star formation history (e.g., Firmani et al. 2004; Pescalli et al. 2016; Wanderman & Piran 2010), the need for including the time delay effect when simulating the short GRB redshift distribution is essential. This is supported by many works, for example, Ando (2004), Gal-Yam et al. (2008), Guetta & Piran (2006), Guetta & Stella (2009), Mészáros et al. (2006), Nakar et al. (2006), and Wanderman & Piran (2015). The time delay distribution is usually approximated with a Gaussian or a lognormal model (e.g., Sun et al. 2015). We used the formulae of Sun et al. (2015) to simulate the redshift distribution for our kilonova samples (Equations 20 and 21 in Sun et al. (2015)).

However, since the brightness of the kilonova afterglows allow them to be observed only up to moderate redshifts ($z \lesssim 0.1$), it is also a common practice to neglect the effect arising from the redshift (e.g., Saleem et al. 2018a; Scolnic et al. 2018; Wollaeger et al. 2018). Thus, we also generate a light curve sample where the redshift to the events is distributed uniformly for both the V17 and P17 model (the corresponding distance interval is between 100 and 740 Mpc).

2.3 | Binary neutron star merger rate

The double neutron star merger rates can be inferred with two different methods: determining the rate from short GRB observations or calculating it by employing binary compact object population synthesis methods. The former method is less reliable, since it is believed to suffer from the uncertainties of various parameters, like the beaming factor, redshift, minimum luminosity, and the time-delay distribution. If we assume that *all* of the short GRBs produce KNe, then the rate lies between 0.2 (Ghirlanda et al. 2016) and 40 $\rm Gpc^{-3}\ yr^{-1}$ per $f_{\rm b}^{-1} = 1 - \cos\theta_{\rm j}$ (Nakar et al. 2006), where $f_{\rm b}$ is the beaming factor and $\theta_{\rm j}$ is the jet half-opening angle. Much higher KNe afterglow rate can be derived if we assume that *all* of the binary neutron star merger events result in KNe, namely as high as 1540 $\rm Gpc^{-3}\ yr^{-1}$ (Abbott et al. 2017a).

3 | RESULTS

Having the simulated KNe afterglow sample, we can now determine the expected KNe afterglow rate and compare these rates in the light of the different models.

3.1 | Merger time delay models

As it can be seen in Figure 1, the distributions of the maximum brightness of samples with lognormal and Gaussian time delay models in the case of the P17 model shows only a small discrepancy. However, the expected rate for the Gaussian model is higher for both the V17 and P17 models. The higher afterglow rate produced by the Gaussian time delay model can be interpreted with the shape of the distribution: there are simply more bursts with shorter time delays compared with the logarithmic case.

3.2 | Uniform versus observed redshift distribution

In agreement with the presumptions that the redshift effects can be neglected when simulating KNe afterglows in our vicinity (e.g., Saleem et al. 2018a) our results show that in the case of the spherical V17 model, there is no discrepancy in the predicted number of afterglows generated with the observed and uniform redshift distributions. However, the axisymmetrical P18 model produces 30% more observable afterglows compared with the case when we applied the observed redshift distribution.

3.3 | Spherical versus axisymmetrical model

The spherical V17 model has two main drawbacks compared with the more sophisticated axisymmetrical P17 model: (a)

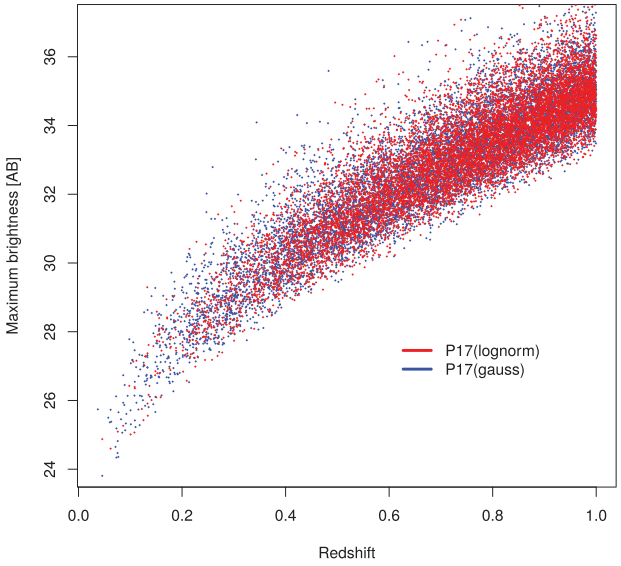

FIGURE 1 The figure shows the maximum brightness distribution against the redshift in the cases of a lognormal and Gaussian time delay models. Although, there is no difference in the shape of the distributions, the Gaussian model produces brighter afterglows at lower redshifts ($z \lesssim 0.4$)

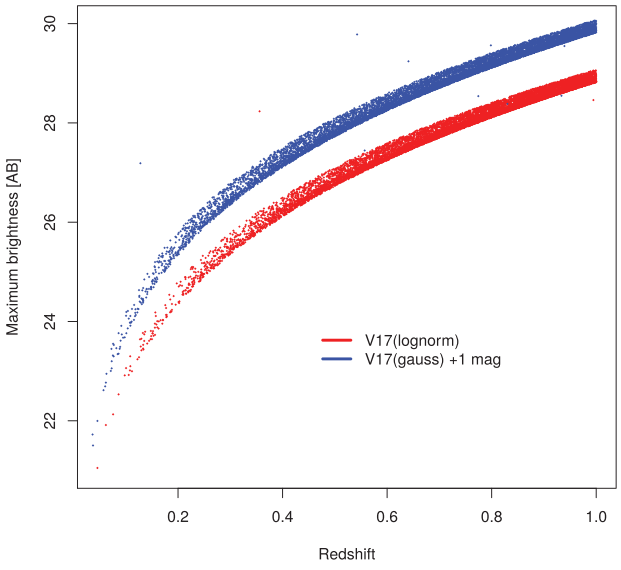

FIGURE 2 The plot shows that allowing only the ejecta mass to vary in the V17 model results in a very narrow maximum brightness distribution. Also, there is no difference between the Gauss and lognormal time delay models. For clarity, the distributions are separated on the plot

the spherical structure is unable to appropriately describe the angular alignment of the progenitor star and (b) allowing only the mass to vary (as was done by Cowperthwaite et al. (2019)) results in a very narrow brightness distribution. This can be observed in Figure 2, where we plotted the maximum afterglow brightness against the redshift. This effect can be seen also in Figure 3, where the histograms of the maximum afterglow brightness of the P17 and V17 samples are shown. The first effect can lead to incorrect predictions for

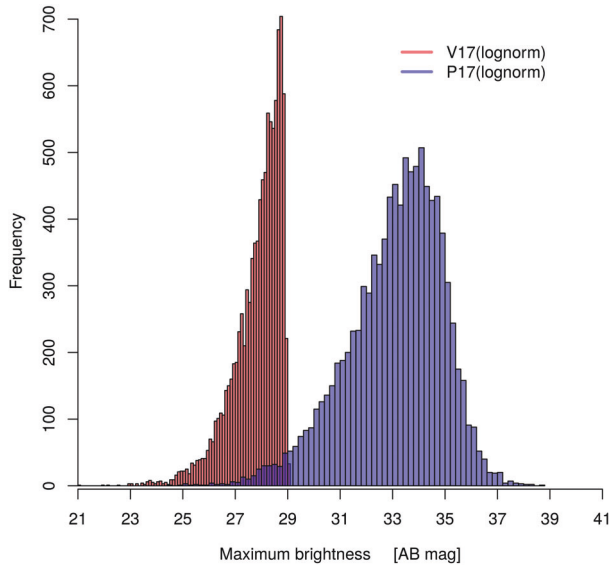

FIGURE 3 This histogram compares the maximum brightness of afterglow samples generated with the spherical and the axisymmetrical models described in Section 2.1. Of course, only a qualitative comparison can be done since not only the physical configuration of the models are different, but the input parameters are chosen from a distinct intervals

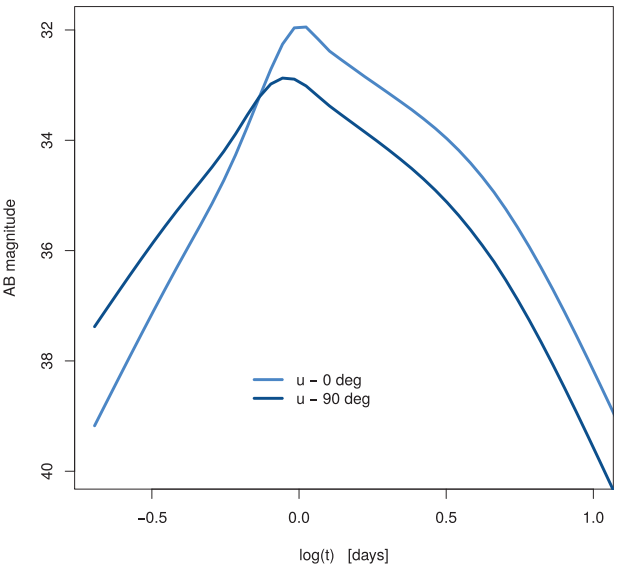

FIGURE 4 The structure of the ejecta can have a significant effect on the light curce shape and the brightness: radiation coming from a polar dominated blue ejecta may be obscured if the line of sight is in the equatorial plane of the remnant

the rate, since, for example, the radiation coming from an otherwise obscured ejecta component might be overestimated, or similarly, underestimated. This can be clearly seen in Figure 4.

3.4 | Uncertainties in the cosmological parameters

Recently, some results emerged concerning about the value of the Hubble constant, H_0, (Riess et al. 2019, 2016).

TABLE 2 The estimated kilonova afterglow detection rate (event/year) for LSST up to $z \leq 1$

Model	*u*	*g*	*r*	*i*	*z*	*Y*
V17 (log)	1	18	18	14	8	1
V17 (Gauss)	1	18	36	14	8	1
P17 (log)	0	0	<1(6)	<1(11)	<1(6)	0
P17 (Gauss)	0	<1(11)	1(44)	1(55)	1(44)	<1(11)

Note: The contrast in the expected number of afterglows is significant. While the spherical model can produce up to ∼36 detectable afterglows per year, the axisymmetric model generates only ∼1 observable kilonova observation every year. The numbers in the brackets correspond to the case when we assume that *all* of the binary neutron star merger events results in a kilonova.

Riess et al. (2019) with the help of Cepheid variables calculated the Hubble constant from SN Ia measurements: $H_0 = 74.2 \pm 3.6$ km s^{-1} Mpc^{-1}. Adding more Cepheid variables and Ia type SNe, this value was further refined to have only 1.3% of uncertainty: $H_0 = 74.03 \pm 1.42$ km s^{-1} Mpc^{-1}. For the discrepancy between the results of the *Planck* high-redshift measurements ($H_0 = 67.8$ km s^{-1} Mpc^{-1}) and their results, they give a possible explanation that an additional source of dark radiation was present in the early Universe (Poulin et al. 2019). The larger value of the Hubble constant is already supported by other works, for example, Burns et al. (2018), Dhawan et al. (2018), and Feeney et al. (2018). On the other hand, some authors using measurements of the Baryonic Acoustic Oscillation and Ia type SNe/primordial deuterium abundance determined the Hubble constant to be $H_0 \approx 66.98 - 67.8$ km s^{-1} Mpc^{-1} (Addison et al. 2018; Macaulay et al. 2019). Thus, beacuse of the unsettled value of the Hubble constant, we generate afterglow sample not just with the value determined from the Planck experiment but with the one calculated by Riess et al. (2019).

In addition to the Hubble tension, the uncertainties of the Ω_M and Ω_Λ parameters are still a matter of debate. Mészáros (2002) applying statistical tests to the sample from Perlmutter et al. (1999) proved that the null hypothesis of the zero cosmological constant can not be rejected based on Ia SN data. By reanalyzing the data supporting the $\Lambda > 0$ model, Rowan-Robinson (2002) came to the conclusion that the host galaxy extinction of Ia SNe was underestimated implying that the direct evidence from Ia SNe for the positive Λ is inconclusive. The results of Tonry et al. (2003), who determined the distances and host galaxy extinctions for 230 Ia SNe, also support the $\Omega_\Lambda = 0$ hypothesis. Similar to Rowan-Robinson (2002), Hetesi & Balázs (2005) also suggested that the host galaxy extinction measurements of Ia SNe used for calculating the value of Ω_Λ may be incorrect making the determination of Ω_Λ unreliable. Balázs et al. (2006) found a possible interrelation between the luminosity distances and internal extinctions of Ia type SNe. After correcting the luminosity distances, they came to the conclusion that the SN Ia data alone cannot exclude the possibility of $\Lambda = 0$. A recent numerical simulation by Rácz et al. (2017) with an initial $\Omega_M = 1$ can track the structure growth of the ΛCDM cosmology remarkably well. Because of the above-mentioned results, we simulated an afterglow sample with the spherical model using the latest value of the Hubble constant, and another one where we set $\Omega_\Lambda = 0$ in addtion. However, the number of predicted kilonova afterglows with $H_0 = 74.03 \pm 1.42$ km s^{-1} Mpc^{-1}, and $\Omega_\Lambda = 0.692$ is exactly the same as in the case of the samples generated with $H_0 = 67.8$ km s^{-1} Mpc^{-1}. Moreover, if Ω_Λ is set to 0, then the rate is greater by 20% compared with the case with $\Omega_\Lambda = 0.692$.

3.5 | Expected kilonova rate for LSST

If we take the maximum central value (40) of the short GRB rates from table 2 in Della Valle et al. (2018), the corresponding rate for $z \leq 1$ is ∼6,555 event/year if $f_b^{-1} = 1$ (where $f_b^{-1} = 1 - \cos\theta$, and θ is the jet half-opening angle). If we assume that *all* binary neutron star merger system results in a KNe event, then the rate is ∼ 250,000 event/year.

In this article, we do not attempt to simulate the" real" Large Synoptic Survey Telescope (LSST) cadence (i.e., taking into account the effects of airmass, seeing, and sky brightness), since we are interested only in the relative afterglow rate regarding the different models. Taking the nominal survey area of 18,000 deg^2 and the LSST single-visit 5-σ limiting depths for point sources m_5 = (23.7, 24.9, 24.4, 24.0, 23.5, and 22.6) in the (u, g, r, i, z, and y) bands (Ivezić et al. 2019), we consider a successful detection when the afterglow reaches the detection limit in at least one band. Table 2 summarizes the expected kilonova detection rates for the different models. As it can be inspected from this table, the spherical model produces significantly higher afterglow detection rates.

4 | CONCLUSIONS

In this paper, we simulated KNe afterglows following double neutron star merger events. In order to investigate the effect of the structural compositon on the underlying physical model, we created afterglow samples with spherical and axisymmetrical models. Our results show the following:

1 There is a significant difference in the expected kilonova rate between the spherical and axisymmetrical models (∼36 vs. ∼1, respectively).
2 The afterglow sample simulated with the observed redshift distribution and the spherical model predicts the same number of observable afterglows than the sample generated with the uniform redshift distribution in volume; however, the axisymmetrical model with the uniform redshift distribution in volume results in 30% more detectable afterglows compared with the case with the observed redshift distribution.
3 Afterglows with spherical ejecta structure can be detected up to $z \lesssim 1$.
4 Using the latest calculated value of H_0 ($74.03 \pm 1.42\,\mathrm{km\,s^{-1}\ Mpc^{-1}}$), the estimated number of observable afterglows simulated with the spherical model does not change compared with the case where we use $H_0 = 67.8\,\mathrm{km\,s^{-1}\,Mpc}$; however, if we replace $\Omega_\Lambda = 0.692$ with $\Omega_\Lambda = 0$ in addition, the rate becomes higher by 20% (which should be taken as a lower limit for the axisymmetrical model). These discrepancies being so small most likely can be explained by the fact that kilonova afterglows are detectable only at lower redshifts ($z < 1$).

Based on the above-mentioned results, we conclude that the axisymmetrical model is much sensitive to the values of the input parameters which can be explained by the fact that it is more complex. However, this does not mean necessarily that the spherical model is less reliable. Nevertheless, since the afterglow rates inferred from various methods still cover a very wide range of values, the ultimate test for the kilonova afterglow rate will be carried out by the upcoming sky surveys.

ACKNOWLEDGMENT

We kindly thank the anonymous referee for the valuable suggestions which significantly improved the quality of this paper.

CONFLICT OF INTERESTS

The authors declare no potential conflict of interests.

REFERENCES

Abbott, B. P., Abbott, R., Abbott, T. D., et al. 2017a, *ApJ*, *848*, L12. https://doi.org/10.3847/2041-8213/aa91c9.

Abbott, B. P., Abbott, R., Abbott, T. D., et al. 2017b, *ApJ*, *848*, L13. https://doi.org/10.3847/2041-8213/aa920c.

Addison, G. E., Watts, D. J., Bennett, C. L., Halpern, M., Hinshaw, G., & Weiland, J. L. 2018, *ApJ*, *853*(2), 119. https://doi.org/10.3847/1538-4357/aaa1ed.

Ando, S. 2004, *J. Cosmol. Astropart. Phys.*, *6*, 007. https://doi.org/10.1088/1475-7516/2004/06/007.

Balázs, L. G., Bagoly, Z., Horváth, I., Mészáros, A., & Mészáros, P. 2003, *A&A*, *401*, 129. https://doi.org/10.1051/0004-6361:20021863.

Balázs, L. G., Hetesi, Z., Regály, Z., Csizmadia, S., Bagoly, Z., Horváth, I., & Mészáros, A. 2006, *Astronomische Nachrichten*, *327*(9), 917. https://doi.org/10.1002/asna.200610649.

Belczynski, K., Repetto, S., Holz, D. E., et al. 2016, *ApJ*, *819*, 108. https://doi.org/10.3847/0004-637X/819/2/108.

Bloom, J. S., Kulkarni, S. R., Price, P. A., et al. 2002, *ApJ*, *572*(1), L45. https://doi.org/10.1086/341551.

Bogomazov, A. I., Lipunov, V. M., & Tutukov, A. V. 2007, *Astron. Rep.*, *51*(4), 308. https://doi.org/10.1134/S1063772907040063.

Burns, C. R., Parent, E., Phillips, M. M., et al. 2018, *ApJ*, *869*(1), 56. https://doi.org/10.3847/1538-4357/aae51c.

Cao, X.-F., Yu, Y.-W., & Zhou, X. 2018, *ApJ*, *858*, 89. https://doi.org/10.3847/1538-4357/aabadd.

Christensen, L., Hjorth, J., & Gorosabel, J. 2004, *A&A*, *425*, 913. https://doi.org/10.1051/0004-6361:20040361.

Chruslinska, M., Belczynski, K., Klencki, J., & Benacquista, M. 2018, *MNRAS*, *474*, 2937. https://doi.org/10.1093/mnras/stx2923.

Coward, D. M., Howell, E. J., Piran, T., et al. 2012, *MNRAS*, *425*(4), 2668. https://doi.org/10.1111/j.1365-2966.2012.21604.x.

Cowperthwaite, P. S., Villar, V. A., Scolnic, D. M., & Berger, E. 2019, *ApJ*, *874*(1), 88. https://doi.org/10.3847/1538-4357/ab07b6.

Della Valle, M., Guetta, D., Cappellaro, E., et al. 2018, *MNRAS*, *481*, 4355. https://doi.org/10.1093/mnras/sty2541.

Dhawan, S., Jha, S. W., & Leibundgut, B. 2018, *A&A*, *609*, A72. https://doi.org/10.1051/0004-6361/201731501.

Dietz, A. 2011, *A&A*, *529*, A97. https://doi.org/10.1051/0004-6361/201016166.

Dominik, M., Belczynski, K., Fryer, C., et al. 2013, *ApJ*, *779*, 72. https://doi.org/10.1088/0004-637X/779/1/72.

Eichler, D., Livio, M., Piran, T., & Schramm, D. N. 1989, *Nature*, *340*(6229), 126. https://doi.org/10.1038/340126a0.

Eldridge, J. J., Stanway, E. R., & Tang, P. N. 2019, *MNRAS*, *482*, 870. https://doi.org/10.1093/mnras/sty2714.

Feeney, S. M., Mortlock, D. J., & Dalmasso, N. 2018, *MNRAS*, *476*(3), 3861. https://doi.org/10.1093/mnras/sty418.

Firmani, C., Avila-Reese, V., Ghisellini, G., & Tutukov, A. V. 2004, *ApJ*, *611*(2), 1033. https://doi.org/10.1086/422186.

Fox, D. B., Frail, D. A., Price, P. A., et al. 2005, *Nature*, *437*(7060), 845. https://doi.org/10.1038/nature04189.

Gal-Yam, A., Nakar, E., Ofek, E. O., et al. 2008, *ApJ*, *686*(1), 408. https://doi.org/10.1086/590947.

Galama, T. J., Vreeswijk, P. M., van Paradijs, J., et al. 1998, *Nature*, *395*(6703), 670. https://doi.org/10.1038/27150.

Gehrels, N., Sarazin, C. L., O'Brien, P. T., et al. 2005, *Nature*, *437*, 851. https://doi.org/10.1038/nature04142.

Ghirlanda, G., Salafia, O. S., Pescalli, A., et al. 2016, *A&A*, *594*, A84. https://doi.org/10.1051/0004-6361/201628993.

Guetta, D., & Piran, T. 2006, *A&A*, *453*(3), 823. https://doi.org/10.1051/0004-6361:20054498.

Guetta, D., & Stella, L. 2009, *A&A*, *498*(2), 329. https://doi.org/10.1051/0004-6361:200810493.

Guillochon, J., Nicholl, M., Villar, V. A., et al. 2018, *ApJS*, *236*, 6. https://doi.org/10.3847/1538-4365/aab761.

Hetesi, Z., & Balázs, L. G. 2005, *Publ. Astron. Department of the Eotvos Lorand University*, *15*, 159.

Hjorth, J., Sollerman, J., Møller, P., et al. 2003, *Nature*, *423*, 847. https://doi.org/10.1038/nature01750.

Ivezić, Ž., Kahn, S. M., Tyson, J. A., et al. 2019, *ApJ*, *873*(2), 111. https://doi.org/10.3847/1538-4357/ab042c.

Jin, Z.-P., Li, X., Cano, Z., Covino, S., Fan, Y.-Z., & Wei, D.-M. 2015, *ApJ*, *811*, L22. https://doi.org/10.1088/2041-8205/811/2/L22.

Jin, Z.-P., Li, X., Wang, H., et al. 2018, *ApJ*, *857*, 128. https://doi.org/10.3847/1538-4357/aab76d.

Kouveliotou, C., Meegan, C. A., Fishman, G. J., et al. 1993, *ApJ*, *413*, L101. https://doi.org/10.1086/186969.

Kruckow, M. U., Tauris, T. M., Langer, N., Kramer, M., & Izzard, R. G. 2018, *MNRAS*, *481*, 1908. https://doi.org/10.1093/mnras/sty2190.

Li, L.-X., & Paczyński, B. 1998, *ApJ*, *507*(1), L59. https://doi.org/10.1086/311680.

Macaulay, E., Nichol, R. C., Bacon, D., et al. 2019, *MNRAS*, *486*(2), 2184. https://doi.org/10.1093/mnras/stz978.

Mapelli, M., & Giacobbo, N. 2018, *MNRAS*, *479*, 4391. https://doi.org/10.1093/mnras/sty1613.

Mészáros, A. 2002, *ApJ*, *580*(1), 12. https://doi.org/10.1086/343071.

Mészáros, A., Bagoly, Z., Balázs, L. G., & Horváth, I. 2006, *A&A*, *455*(3), 785. https://doi.org/10.1051/0004-6361:20053807.

Nakar, E., Gal-Yam, A., & Fox, D. B. 2006, *ApJ*, *650*(1), 281. https://doi.org/10.1086/505855.

Narayan, R., Paczynski, B., & Piran, T. 1992, *ApJ*, *395*, L83. https://doi.org/10.1086/186493.

Paul, D. 2018, *MNRAS*, *477*(4), 4275. https://doi.org/10.1093/mnras/sty840.

Perego, A., Radice, D., & Bernuzzi, S. 2017, *ApJ*, *850*, L37. https://doi.org/10.3847/2041-8213/aa9ab9.

Perlmutter, S., Aldering, G., Goldhaber, G., et al. 1999, *ApJ*, *517*(2), 565. https://doi.org/10.1086/307221.

Pescalli, A., Ghirlanda, G., Salvaterra, R., et al. 2016, *A&A*, *587*, A40. https://doi.org/10.1051/0004-6361/201526760.

Petrillo, C. E., Dietz, A., & Cavaglià, M. 2013, *ApJ*, *767*(2), 140. https://doi.org/10.1088/0004-637X/767/2/140.

Planck Collaboration, Ade, P. A. R., Aghanim, N., et al. 2016, *A&A*, *594*, A13. https://doi.org/10.1051/0004-6361/201525830.

Pol, N., McLaughlin, M., & Lorimer, D. R. 2019, *ApJ*, *870*, 71. https://doi.org/10.3847/1538-4357/aaf006.

Poulin, V., Smith, T. L., Karwal, T., & Kamionkowski, M. 2019, *Phys. Rev. Lett.*, *122*(22), 221301. https://doi.org/10.1103/PhysRevLett.122.221301.

Rácz, G., Dobos, L., Beck, R., Szapudi, I., & Csabai, I. 2017, *MNRAS*, *469*(1), L1. https://doi.org/10.1093/mnrasl/slx026.

Riess, A. G., Casertano, S., Yuan, W., Macri, L. M., & Scolnic, D. 2019, *ApJ*, *876*(1), 85. https://doi.org/10.3847/1538-4357/ab1422.

Riess, A. G., Macri, L. M., Hoffmann, S. L., et al. 2016, *ApJ*, *826*(1), 56. https://doi.org/10.3847/0004-637X/826/1/56.

Rowan-Robinson, M. 2002, *MNRAS*, *332*(2), 352. https://doi.org/10.1046/j.1365-8711.2002.05299.x.

Ruffini, R., Rodriguez, J., Muccino, M., et al. 2018, *ApJ*, *859*(1), 30. https://doi.org/10.3847/1538-4357/aabee4.

Sadowski, A., Belczynski, K., Bulik, T., Ivanova, N., Rasio, F. A., & O'Shaughnessy, R. 2008, *ApJ*, *676*, 1162. https://doi.org/10.1086/528932.

Saleem, M., Pai, A., Misra, K., Resmi, L., & Arun, K. G. 2018a, *MNRAS*, *475*, 699. https://doi.org/10.1093/mnras/stx3108.

Saleem, M., Resmi, L., Misra, K., Pai, A., & Arun, K. G. 2018b, *MNRAS*, *474*(4), 5340. https://doi.org/10.1093/mnras/stx3104.

Scolnic, D., Kessler, R., Brout, D., et al. 2018, *ApJ*, *852*, L3. https://doi.org/10.3847/2041-8213/aa9d82.

Soares-Santos, M., Holz, D. E., Annis, J., et al. 2017, *ApJ*, *848*, L16. https://doi.org/10.3847/2041-8213/aa9059.

Sun, H., Zhang, B., & Li, Z. 2015, *ApJ*, *812*, 33. https://doi.org/10.1088/0004-637X/812/1/33.

Tan, W.-W., Fan, X.-L., & Wang, F. Y. 2018, *MNRAS*, *475*, 1331. https://doi.org/10.1093/mnras/stx3242.

Tanvir, N. R., Levan, A. J., Fruchter, A. S., Hjorth, J., Hounsell, R. A., Wiersema, K., & Tunnicliffe, R. L. 2013, *Nature*, *500*(7464), 547. https://doi.org/10.1038/nature12505.

Tonry, J. L., Schmidt, B. P., Barris, B., et al. 2003, *ApJ*, *594*(1), 1. https://doi.org/10.1086/376865.

Vigna-Gómez, A., Neijssel, C. J., Stevenson, S., et al. 2018, *MNRAS*, *481*, 4009. https://doi.org/10.1093/mnras/sty2463.

Villar, V. A., Guillochon, J., Berger, E., et al. 2017, *ApJ*, *851*, L21. https://doi.org/10.3847/2041-8213/aa9c84.

Virgili, F. J., Mundell, C. G., Pal'shin, V., et al. 2013, *ApJ*, *778*(1), 54. https://doi.org/10.1088/0004-637X/778/1/54.

Řípa, J., & Mészáros, A. 2016, *Ap&SS*, *361*(12), 370. https://doi.org/10.1007/s10509-016-2960-4.

Řípa, J., Mészáros, A., Veres, P., & Park, I. H. 2012, *ApJ*, *756*(1), 44. https://doi.org/10.1088/0004-637X/756/1/44.

Wanderman, D., & Piran, T. 2010, *MNRAS*, *406*, 1944. https://doi.org/10.1111/j.1365-2966.2010.16787.x.

Wanderman, D., & Piran, T. 2015, *MNRAS*, *448*, 3026. https://doi.org/10.1093/mnras/stv123.

Wollaeger, R. T., Korobkin, O., Fontes, C. J., et al. 2018, *MNRAS*, *478*, 3298. https://doi.org/10.1093/mnras/sty1018.

Woosley, S. E. 1993, *ApJ*, *405*, 273. https://doi.org/10.1086/172359.

Yang, B., Jin, Z.-P., Li, X., et al. 2015, *Nat. Commun.*, *6*, 7323. https://doi.org/10.1038/ncomms8323.

Yonetoku, D., Nakamura, T., Sawano, T., Takahashi, K., & Toyanago, A. 2014, *ApJ*, *789*(1), 65. https://doi.org/10.1088/0004-637X/789/1/65.

Zhang, G. Q., & Wang, F. Y. 2018, *ApJ*, *852*, 1. https://doi.org/10.3847/1538-4357/aa9ce5.

Ziosi, B. M., Mapelli, M., Branchesi, M., & Tormen, G. 2014, *MNRAS*, *441*(4), 3703. https://doi.org/10.1093/mnras/stu824.

AUTHOR BIOGRAPHY

J. Kóbori received his MSc in astronomy in 2011 (thesis: Observations of gamma ray bursts' afterglows at optical wavelengths) under the supervision of Péter Veres and János Kelemen from Eötvös Loránd University, Budapest, Hungary. He is currently pursuing the Ph.D. degree at the School of Physics (Particle Physics and Astronomy, Eötvös Loránd University) on γ-ray bursts (groups, afterglows, and rates) and kilonovae.

How to cite this article: Kóbori J. Kilonova afterglow rate from spherical and axisymmetrical models. *Astron. Nachr*. 2019;340:586–592. https://doi.org/10.1002/asna.201913660